# University of Groningen

## Coexistence of bulk and surface states probed by Shubnikov–de Haas oscillations in Bi2Se3 with high charge-carrier density

de Vries, Eric; Pezzini, S; Meijer, M.J.; Koirala, N.; Salehi, M. ; Moon, J.; Oh, S. ; Wiedmann, S. ; Banerjee, Tamalika

**IMPORTANT NOTE:** You are advised to consult the publisher's version (publisher's PDF) if you wish to cite from it. Please check the document version below.

*Document Version*
Publisher's PDF, also known as Version of record

*Publication date:*
2017

[Link to publication in University of Groningen/UMCG research database](#)

# Coexistence of bulk and surface states probed by Shubnikov–de Haas oscillations in Bi$_2$Se$_3$ with high charge-carrier density

E. K. de Vries,[1,*] S. Pezzini,[2] M. J. Meijer,[2] N. Koirala,[3] M. Salehi,[4] J. Moon,[3] S. Oh,[3] S. Wiedmann,[2] and T. Banerjee[1,†]

[1]*University of Groningen, Zernike Institute for Advanced Materials, 9747 AG Groningen, The Netherlands*
[2]*High Field Magnet Laboratory (HFML-EMFL) and Institute for Molecules and Materials, Radboud University, 6525 ED Nijmegen, The Netherlands*
[3]*Department of Physics and Astronomy, Rutgers University, Piscataway, New Jersey 08854, USA*
[4]*Department of Materials Science and Engineering, Rutgers University, Piscataway, New Jersey 08854, USA*
(Received 7 March 2017; published 27 July 2017)

Topological insulators are ideally represented as having an insulating bulk with topologically protected, spin-textured surface states. However, it is increasingly becoming clear that these surface transport channels can be accompanied by a finite conducting bulk, as well as additional topologically trivial surface states. To investigate these parallel conduction transport channels, we studied Shubnikov–de Haas oscillations in Bi$_2$Se$_3$ thin films, in high magnetic fields up to 30 T so as to access channels with a lower mobility. We identify a clear Zeeman-split bulk contribution to the oscillations from a comparison between the charge-carrier densities extracted from the magnetoresistance and the oscillations. Furthermore, our analyses indicate the presence of a two-dimensional state and signatures of additional states the origin of which cannot be conclusively determined. Our findings underpin the necessity of theoretical studies on the origin of and the interplay between these parallel conduction channels for a careful analysis of the material's performance.

Topological insulators (TIs), hosting spin-momentum locked surface states, received considerable interest in the past decade potentially serving as a platform for exploring many interesting concepts in physics [1–3]. These surface states have been well investigated by surface sensitive techniques like (spin-)angular resolved photo-emission spectroscopy [4,5] and scanning tunneling microscopy and spectroscopy [6–8]. Such techniques adequately describe the electronic properties of the (non)trivial surface states, but cannot account for additional transport features as observed in (magneto)transport experiments. To employ topological insulators in solid-state devices, direct access and understanding of these additional surface states in transport experiments are needed.

Studying Shubnikov–de Haas (SdH) oscillations can reveal the existence of such surface states where parameters like mobility, charge-carrier density, the dimensionality, and the Berry phase of the states can be determined [2]. Earlier studies on various Bi-based topological insulators report on single or double frequency SdH oscillations [9–22], where it is often claimed that these oscillations originate from the top and bottom topological surface state (TSS) with the expected Berry phase and angular dependence. The magnetic field strength used in these studies is usually up to 15 T, which can only probe transport channels with a relatively high mobility, whereas nonlinear Hall measurements indicate additional channels with a lower mobility to be present. Besides a finite conducting bulk, these additional (topologically trivial) channels can originate from variations in the electrostatic potential near the surfaces and can also be spin textured [23–25], which we will refer to as two-dimensional electron gas (2DEG). From earlier transport measurements, the mobilities of the different channels are found to be on the order of 50–500 and ~3000 cm$^2$(V s)$^{-1}$ where the low mobility channel has a higher charge-carrier

density [16,26]. Notably, from these numbers one can find that in terms of conductivity these channels can contribute equally to the electrical transport.

Motivated by these works, we performed magnetotransport experiments up to 30 T and studied SdH oscillations to explore the most prominent conduction channels and additional channels with mobilities below 1000 cm$^2$(V s)$^{-1}$ ($\mu B \gg 1$, where $\mu$ is the charge mobility and $B$ the applied magnetic field strength). The magnetotransport is studied in thin films of Bi$_2$Se$_3$ so as to minimize bulk effects and amplify the topologically trivial and nontrivial surface states. In contrast to earlier works, we will show that the bulk channel with a high mobility is present along with a prominent two-dimensional (2D) channel which can be linked to the topological surface states. Our findings indicate the presence of additional channels with a lower mobility that cannot be precisely resolved from the oscillations. Similar to Ref. [27], we compare charge-carrier densities from the SdH oscillations as well as from the magnetoresistance and study the dimensionality of the various channels in order to unravel the origin of these states.

In this paper, we used thin films of $n$-type Bi$_2$Se$_3$ with thickness $t = 10$, 20, 30, and 100 quintuple layers (QLs) grown by molecular-beam epitaxy (MBE) on Al$_2$O$_3$(0001) substrates in a custom-designed SVTA MOS-V-2 MBE system at a base pressure lower than $5 \times 10^{-10}$ Torr following the methods as described in previous work [28]. The quality of the obtained films was characterized through various techniques [16,29–32]. The films were patterned into Hall bars by using a combination of photolithography and Ar plasma dry etching. Contact pads consisting of Ti(5)/Au(70 nm) were made by combining photolithography with electron-beam evaporation. The resulting Hall bars [inset Fig. 1(a)] have dimensions of $2400 \times 100$ μm$^2$ where the resistance is measured over a probing length between 1400 and 2000 μm. The magnetotransport measurements have been performed in a cryostat with an out-of-plane rotation stage placed in a 30-T Bitter-type magnet in a four-probe geometry using the ac modulation technique at

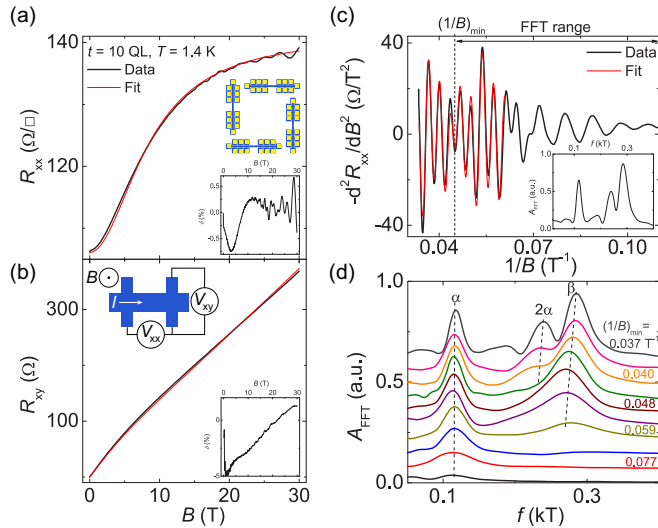*eric.de.vries@rug.nl
†t.banerjee@rug.nl

| $t$ (QL) | $n_1/t$ $(\times 10^{19} \mathrm{cm}^{-3})$ | $n_2$ $(\times 10^{13} \mathrm{cm}^{-2})$ | $\mu_1$ $[\mathrm{cm}^2 (\mathrm{V\,s})^{-1}]$ | $\mu_2$ $[\mathrm{cm}^2 (\mathrm{V\,s})^{-1}]$ |
|---|---|---|---|---|
| $10 \pm 1$ | $1.8 \pm 0.1$ | $3.4 \pm 0.2$ | $2060 \pm 50$ | $660 \pm 50$ |
| $20 \pm 1$ | $0.67 \pm 0.03$ | $2.4 \pm 0.2$ | $1190 \pm 50$ | $290 \pm 50$ |
| $30 \pm 1$ | $0.49 \pm 0.02$ | $2.7 \pm 0.1$ | $1250 \pm 50$ | $220 \pm 50$ |
| $100 \pm 5$ | $0.33 \pm 0.02$ | $4.2 \pm 0.2$ | $3800 \pm 100$ | $500 \pm 100$ |

$= \hat{\sigma}^{-1}$ (more details on the analysis can be found in Ref. [33]):

$$\sigma_{xx} = \frac{n_1 e \mu_1}{1 + \mu_1^2 B^2} + \frac{n_2 e \mu_2}{1 + \mu_2^2 B^2},$$

$$\sigma_{xy} = \frac{n_1 e \mu_1^2 B}{1 + \mu_1^2 B^2} + \frac{n_2 e \mu_2^2 B}{1 + \mu_2^2 B^2}. \quad (1)$$

As found from our analysis, simultaneous fitting of the $R_{xx}$ and $R_{xy}$ is required since $R_{xx}$ has a strong effect on the mobility and therefore will change the values found for $n_i$ from $R_{xy}$. An example of the simultaneous fit to the magnetoresistance curves $R_{xx}$ and $R_{xy}$ for the sample with $t = 10$ QL at 1.4 K is displayed in Fig. 1(a). A good agreement with the two-carrier model is obtained with a residual $\delta = (R_{\mathrm{data}} - R_{\mathrm{fit}})/R_{\mathrm{data}}$ between 1 and 5% for both $R_{xx}$ and $R_{xy}$, but it is important to note that this analysis is limited to two channels and does not rule out the presence of more channels. Nevertheless, the good agreement between data and fit suggests that any additional state would have a similar mobility, which would add to an effective charge-carrier density in Eq. (1).

An overview of the extracted charge-carrier properties for all film thicknesses can be found in Table I; the data and fits to the magnetoresistance for the samples with larger thickness can be found in Ref. [33]. We listed $n_1/t$ because of its correspondence to the [three-dimensional (3D)] bulk channel (see discussion below), whereas $n_2$ is most likely linked to a 2D channel. The model describes the magnetoresistance behavior for $t$ up to 30 QL very well, but deviations from the model are observed for $t = 100$ QL, which will be discussed below. The correspondence between these extracted parameters and the information extracted from the SdH oscillations will be discussed in the remainder of this paper.

The possible presence of additional states can be analyzed by studying the SdH oscillations in $R_{xx}$, provided that the mobility of the channels is high enough [27]. For the sample with $t = 10$ QL, these oscillations can be observed from ~10 T onwards, which indicates that transport channels are present with a mobility on the order of $1000 \mathrm{cm}^2 (\mathrm{V\,s})^{-1}$. This is in agreement with estimates for $\mu_1$ as extracted from the magnetoresistance measurements (see Table I). To analyze the oscillations without the magnetoresistance background, the second derivative $-d^2 R_{xx}/dB^2$ is taken after interpolation and adjacent averaging of the data [33]. By plotting $-d^2 R_{xx}/dB^2$ versus $1/B$, we find an oscillatory pattern that shows additional oscillations from 15 T [~0.067 T$^{-1}$, Fig. 1(c)]. We can follow the development of the oscillations by looking at the evolution of the fast Fourier-transform (FFT) spectrum when taking different ranges starting from 9 T ($\sim 0.11$ T$^{-1}$) towards

FIG. 1. (a) Out-of-plane magnetic field dependence of the longitudinal sheet resistance $R_{xx}$ and (b) the Hall resistance $R_{xy}$ for $t = 10$ QL at $T = 1.4$ K. The data (black) can be fitted with the two channel model (red) in good agreement. Oscillations in $R_{xx}$ are clearly visible beyond 15 T. Insets (a): Residual $\delta$ vs magnetic field and Hall bar geometry with TI channel in blue and contact pads in yellow. Inset (b): Residual $\delta$ vs magnetic field. (c) The second derivative of the resistance with respect to the magnetic field $-d^2 R_{xx}/dB^2$ plotted vs $1/B$. A clear oscillatory pattern is present with multiple oscillations. Beyond 15.5 T (0.065 T$^{-1}$) the oscillatory pattern can be reconstructed from oscillations with $f_\alpha = 0.122 \pm 0.003$ kT, $f_{2\alpha} = 0.236 \pm 0.003$ kT, and $f_\beta = 0.291 \pm 0.001$ kT. Inset: Resulting FFT spectrum of the full oscillatory pattern. (d) Magnetic field evolution of the (smoothed) FFT spectrum analyzed for different FFT ranges starting from 11 T towards higher fields with steps of 2 T, as schematically depicted in (c). The FFT amplitude $A_{\mathrm{FFT}}$ is plotted vs frequency $f$ where the curves are offset by 0.07 for clarity.

an ac current bias of 1 μA. In this paper, mainly the results on the sample with $t = 10$ QL will be discussed and comparisons will be made to the samples with larger thickness. Most of the results of the thicker samples can be found in Ref. [33].

The typical out-of-plane magnetic field dependence of the longitudinal sheet resistance $R_{xx}$ measured for the sample with $t = 10$ QL is shown in Fig. 1(a) where $R_{xx}$ tends to saturate at high magnetic fields. From this data and those for larger thickness as well as from the fitting (see below), we observe that the order of saturation is determined by the low mobility channel and the parabolic response at low fields is governed by the high mobility channel. Furthermore, the presence of at least two channels is clear from the nonlinear Hall resistance $R_{xy}$ [Fig. 1(b)]. As also shown earlier [30], we observe a slight upturn with a change in $R_{xx}$ ~0.2% for samples with $t = 10$–30 QL below 10 K, indicative of the presence of defect states [10,12,34]. From the out-of-plane field dependence of the longitudinal and transverse resistance $R_{xx}(B)$ and $R_{xy}(B)$, we can extract the sheet carrier density $n_i$ and mobility $\mu_i$ for only two channels, which we expect to be due to the bulk and surface state(s). For that, we use a semiclassical Drude model where contributions from two parallel channels are summed in the conductivity tensor $\hat{\sigma}$, which relates to the resistivity as $\hat{\rho}$
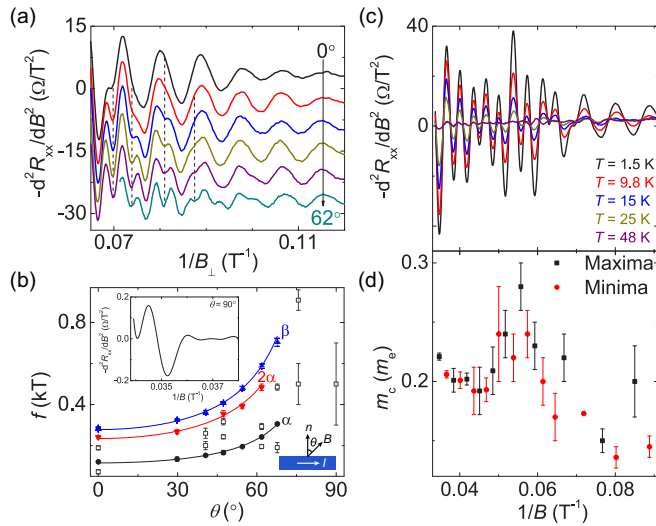
FIG. 2. (a) $B_\perp$ dependence on the oscillations above 0.06 T$^{-1}$ for increasing angle $\theta$ as defined in the inset in (b). An enhancement of the oscillation amplitude is observed at locations indicated by the dashed lines. (b) Angular dependence of the frequencies extracted from the obtained FFT spectra. The dark gray, open square symbols designate additional peaks observed in the FFT spectra but which do not follow a clear angular dependent trend. The large error bars above 70° display the range of the peak position which cannot be determined accurately from the FFT spectrum. Insets: Remaining oscillation at $\theta = 90°$ and schematics of the relative directions of current $I$ and magnetic field $B$. (c) Temperature dependence of the oscillations measured from 1.5 to 48 K. (d) Extracted cyclotron masses per peak position following from the data in (c).

higher fields, where lower mobility channels start to contribute [Fig. 1(d)]. Below 15 T, as depicted by the black, red, and blue line in Fig. 1(d), one main frequency is observed indicated by $\alpha$ in the FFT spectrum as has been commonly reported in other works [11–13,15–17,19,20].

Beyond 15 T, we find the clear presence of the harmonic $2\alpha$ in the FFT spectrum which is due to the strong Zeeman splitting because of the large $g$ factor in this material [35–38]. As shown in Fig. 2(a), the occurrence of Zeeman splitting is justified by an enhancement in oscillation amplitude when studying its dependence on the perpendicular to the in-plane component of the magnetic field, $B_\perp$. Only the cyclotron energy is sensitive to this component, whereas the competing Zeeman energy is related to the total applied magnetic field. In addition to the high mobility channel linked to $\alpha$, we find a lower mobility channel denoted by $\beta$. The appearance of the oscillation linked to $\beta$ at higher magnetic field indicates that this channel has a mobility on the order of several times 100 cm$^2$(V s)$^{-1}$ which is in agreement with the lower value $\mu_2$ found from the earlier analysis of the magnetoresistance (Table I). Using the extracted three frequencies, we can reconstruct the oscillatory pattern at high fields as shown in Fig. 1(c) with deviations in the peak amplitudes of the pattern. Due to the good agreement between data and the reconstructed oscillatory pattern, we can conclude that in the used magnetic field range the magnetotransport is dominated by these three frequencies. Nevertheless, additional channels with a lower mobility might be present but are beyond the resolution of our measurements.

To explore the dimensionality of the observed conduction channels, we can look at the angular dependence of the magnetic field orientation on the position of the frequency peaks. For 2D states we expect that their frequencies $f$ scale with $f \propto 1/\cos\theta$ where $\theta$ is the angle between the surface normal and the direction of the applied magnetic field [inset Fig. 2(b)]. For bulk states it is commonly observed that $f(\theta)$ initially follows the similar behavior but saturates between 30 and 60°, depending on the dimensions of the ellipsoidal pocket of these states [10,18,22,39,40]. However, few earlier works [11,15,41] report on a similar $1/\cos\theta$ dependence for the bulk states as well. Importantly, although we use thin films, the bulk will not show 2D behavior due to finite film thickness since the magnetic length $l_B = \sqrt{\hbar/eB} \leqslant 8$ nm at fields of 10 T from which we start observing the oscillations. From these considerations for $f(\theta)$ we can map out all observed peaks in the spectra at every angle $\theta$ and check whether they fit into a 2D or 3D picture. In Fig. 2(b), the angular dependence of the observed peaks for $t = 10$ QL is plotted from where we can trace the different channels $\alpha$, $2\alpha$, and $\beta$ up to an angle of 68°. Beyond this angle, the resolution of separate spectral peaks is limited, which is most probably linked to the low mobility of the channels and is manifested as a strong weakening of the oscillations at higher angles. Nevertheless, partially due to a higher mobility of the channel, we find a minor oscillation with $f = (0.5 \pm 0.2)$ kT at $\theta = 90°$ indicating that $f_\alpha$ (and its harmonic) saturates and is due to the bulk channel with an elongated Fermi pocket. For the $\beta$ peak, we find a $1/\cos\theta$ behavior which can be linked to the appearance of a 2D state.

Another way of clarifying the origin of the states is to extract the cyclotron mass from the temperature dependence of the oscillations which are observable up to ~50 K as shown in Fig. 2(c). Because of the presence of multiple oscillations it is difficult to extract the cyclotron mass from the FFT spectra. Inspired by recent work [42], we can extract the cyclotron mass by studying the temperature dependence of the peak amplitudes in the oscillations via the Lifshitz-Kosevich formalism. The result is shown in Fig. 2(d) where we can study the evolution of the cyclotron mass upon varying the magnetic field where different oscillations contribute. Comparing this result with the FFT spectrum evolution in Fig. 1(d) in which we observe a single channel up to 0.07 T$^{-1}$, we can conclude that the channel corresponding to the $\alpha$ peak has a cyclotron mass $m_c = (0.15 \pm 0.01)m_e$ which is a typical value for the bulk conduction band [9]. Below 0.07 T$^{-1}$, we find a strong increase in the cyclotron mass up to ~$0.28m_e$ after which it lowers to $(0.20 \pm 0.01)m_e$ and saturates. This higher value of $m_c$ is probably due to the topological surface states [43], whereas a trivial 2DEG is supposed to have a similar mass as the bulk [23]. The interplay of the different oscillations could give rise to an increase in the cyclotron mass because channels with lower mobility ($\propto 1/m_c$) start contributing, provided that the scattering times in the different channels are the same [42].

From the considerations above, we can match the charge-carrier densities extracted from the oscillations and from the magnetoresistance. From the FFT spectrum progression analysis, we can conclude that the $\alpha$ peak makes up the high mobility channel where the charge-carrier density $n_\alpha = (1.26 \pm 0.06) \times 10^{19}$cm$^{-3}$ when assuming bulk states ($n_{3D} = k_{F,b}^2 k_{F,c}/3\pi^2$) with an ellipsoid pocket with ellipticity
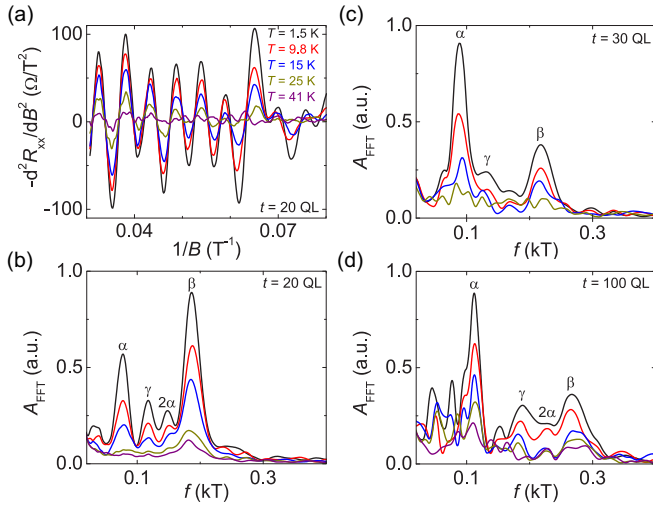
FIG. 3. (a) The second derivative of the resistance with respect to the magnetic field $-d^2R_{xx}/dB^2$ plotted vs $1/B$ for $t = 20$ QL. A clear oscillatory pattern is present with multiple oscillations. (b) Temperature dependence of the FFT spectrum (smoothed) based on the oscillations in (a). Colors correspond to the temperatures as depicted in (a). Temperature-dependent FFT spectra (smoothed) for (c) $t = 30$ QL and (d) $t = 100$ QL.

$k_{F,c}/k_{F,b} = 1.8$ [10]. The value for $n_\alpha$ is in reasonable agreement with $n_1/t$ found from the magnetoresistance analysis (Table I). Furthermore, due to reduced scattering compared to that at any of the surfaces it is most likely that the high mobility channel corresponds to the unaffected bulk layer.

The state indicated by $\beta$ appears above 15 T and thus it is conceivable that this state is linked to the low mobility channel with $n_2$. The origin of the observed 2D surface state, trivial or nontrivial, cannot be concluded from the determination of the Berry phase [33], but the extracted $m_c$ at high fields hints at a topological surface state. Furthermore, it is not clear whether this state resides at the top or bottom surface because the characteristics of the electrostatics at both surfaces are unknown, which would affect the mobility. Assuming $n_{TSS} = k_F^2/4\pi$ for a topological surface state and $n_{2DEG} = k_F^2/2\pi$ for a possible 2DEG, the charge-carrier density related to $f_\beta$ varies between $n_{\beta,TSS} = (6.7 \pm 0.3) \times 10^{12} \text{cm}^{-2}$ and $n_{\beta,2DEG} = (1.34 \pm 0.05) \times 10^{13} \text{cm}^{-2}$, which makes up for 20 or 40% of $n_2$. We are careful to assume that this oscillation is linked to one surface state since it has been earlier reported that similar $n_\beta$ is present at the opposite surface [44], provided the mobilities at both surfaces are similar. Furthermore, as will be shown for $t = 20$ QL, an additional peak between $\alpha$ and $2\alpha$ occurs which shows that additional states exist, which adds to the low mobility charge-carrier density $n_2$.

The picture based on the charge-carrier densities for $t = 10$ QL also applies for the samples with $t = 20$ and 30 QL, but the correction for the ellipsoidal asymmetry is most probably smaller compared to the sample with $t = 10$ QL which can be related to a lower charge-carrier density [10]. Comparing the two films with $t = 10$ and 20 QL, we observe oscillations [Fig. 3(a)] with a similar spectrum but with the presence of an additional $\gamma$ peak [Fig. 3(b)], which could be a signature of a state at the surface opposite to where the channel linked to $\beta$

resides. Furthermore, the peak positions have changed, which is due to differences in charge-carrier density as also observed in the magnetoresistance measurements. From the similarities between these two samples, we can conclude that the thickness (i.e., bulk size) does not play a role but it is rather the relative mobilities and charge-carrier densities in these samples which are the decisive factors for the relative channel contributions.

For the thicker samples, as shown in Figs. 3(c) and 3(d), we observe a dominant peak $\alpha$ in the spectrum while the $2\alpha$, $\beta$, and $\gamma$ peaks are present but with a poor resolution. The reason for the decrease in amplitude is a lower signal-to-noise level of the measured voltage which generates a background and gives rise to a larger spectral width in the FFT spectrum. Furthermore, the oscillations show a beating pattern where oscillations of different frequencies partially cancel each other, yielding a loss of FFT amplitude. For the sample with $t = 100$ QL, we find a poor agreement between the charge-carrier densities from the magnetoresistance and the SdH oscillations where the bulk state ($\alpha$ channel) can alone account for the total charge-carrier density $n_1 + n_2$. The fitting of the magnetoresistance data shows that the mobilities and charge-carrier densities could be different from the extracted values as stronger oscillations were expected for the mobilities extracted. The difference between the fit and data could originate from additional channels with a more distinct mobility suggesting that the two-channel model is too limited to describe the data properly. Lastly, from atomic force microscopy (AFM) images [33] we observe height variations across the film surface, which might influence fitting parameters such as the effective thickness of the transport channel and can cause changes to the bulk density $n_1/t$ on the order of $2 \times 10^{17} \text{cm}^{-3}$. This is in the same range of charge-carrier densities found for the 2D states.

In conclusion, we find a good agreement between magnetoresistance data and the analysis of the SdH oscillations for $Bi_2Se_3$ thin films based on the extracted charge-carrier densities, where the channel contributions are quite unrelated to film thickness. We find that the bulk channel has a high mobility and is characterized by an ellipsoid Fermi pocket but a clear saturation in the angular dependence is absent. Due to the strong $g$ factor in these materials we observe a Zeeman splitting in our oscillations which has been observed before in optical measurements and investigations on thermoelectric effects under high magnetic field. Furthermore, we observe a pronounced 2D state, either topologically trivial or nontrivial, which partially accounts for the low mobility channel's charge-carrier density. Additional 2D states are observed but are often masked by the limited resolution of our analysis originating from the channel mobilities and charge-carrier densities. The limited resolution of the angular dependence and the difficulties to extract parameters like the Berry phase make it difficult to make a definitive statement on the origin of these states.

---

[1] M. Z. Hasan and C. L. Kane, Rev. Mod. Phys. **82**, 3045 (2010).

[2] Y. Ando, J. Phys. Soc. Jpn. **82**, 102001 (2013).

[3] J. E. Moore, Nature (London) **464**, 194 (2010).

[4] Y. Xia, D. Qian, D. Hsieh, L. Wray, A. Pal, H. Lin, A. Bansil, D. Grauer, Y. S. Hor, R. J. Cava, and M. Z. Hasan, Nat. Phys. **5**, 398 (2009).

[5] D. Hsieh, Y. Xia, D. Qian, L. Wray, J. H. Dil, F. Meier, J. Osterwalder, L. Patthey, J. G. Checkelsky, N. P. Ong, A. V. Fedorov, H. Lin, A. Bansil, D. Grauer, Y. S. Hor, R. J. Cava, and M. Z. Hasan, Nature (London) **460**, 1101 (2009).

[6] Z. Alpichshev, J. G. Analytis, J.-H. Chu, I. R. Fisher, Y. L. Chen, Z. X. Shen, A. Fang, and A. Kapitulnik, Phys. Rev. Lett. **104**, 016401 (2010).

[7] P. Roushan, J. Seo, C. V. Parker, Y. S. Hor, D. Hsieh, D. Qian, A. Richardella, M. Z. Hasan, R. J. Cava, and A. Yazdani, Nature (London) **460**, 1106 (2009).

[8] T. Hanaguri, K. Igarashi, M. Kawamura, H. Takagi, and T. Sasagawa, Phys. Rev. B **82**, 081305 (2010).

[9] H. Köhler, Phys. Status Solidi B **58**, 91 (1973).

[10] V. A. Kulbachinskii, N. Miura, H. Nakagawa, H. Arimoto, T. Ikaida, P. Lostak, and C. Drasar, Phys. Rev. B **59**, 15733 (1999).

[11] J. G. Analytis, J.-H. Chu, Y. Chen, F. Corredor, R. D. McDonald, Z. X. Shen, and I. R. Fisher, Phys. Rev. B **81**, 205407 (2010).

[12] N. P. Butch, K. Kirshenbaum, P. Syers, A. B. Sushkov, G. S. Jenkins, H. D. Drew, and J. Paglione, Phys. Rev. B **81**, 241301 (2010).

[13] Z. Ren, A. A. Taskin, S. Sasaki, K. Segawa, and Y. Ando, Phys. Rev. B **82**, 241306 (2010).

[14] M. Petrushevsky, E. Lahoud, A. Ron, E. Maniv, I. Diamant, I. Neder, S. Wiedmann, V. K. Guduru, F. Chiappini, U. Zeitler, J. C. Maan, K. Chashka, A. Kanigel, and Y. Dagan, Phys. Rev. B **86**, 045131 (2012).

[15] B. J. Lawson, Y. S. Hor, and L. Li, Phys. Rev. Lett. **109**, 226406 (2012).

[16] N. Bansal, Y. S. Kim, M. Brahlek, E. Edrey, and S. Oh, Phys. Rev. Lett. **109**, 116804 (2012).

[17] L. Fang, Y. Jia, D. J. Miller, M. L. Latimer, Z. L. Xiao, U. Welp, G. W. Crabtree, and W.-K. Kwok, Nano Lett. **12**, 6164 (2012).

[18] F. Qu, C. Zhang, R.-R. Du, and L. Lu, J. Low Temp. Phys. **170**, 397 (2013).

[19] K. Shrestha, V. Marinova, B. Lorenz, and P. C. W. Chu, Phys. Rev. B **90**, 241111 (2014).

[20] T. R. Devidas, E. P. Amaladass, S. Sharma, R. Rajaraman, D. Sornadurai, N. Subramanian, A. Mani, C. S. Sundar, and A. Bharathi, Europhys. Lett. **108**, 67008 (2014).

[21] C. Zhang, X. Yuan, K. Wang, Z.-G. Chen, B. Cao, W. Wang, Y. Liu, J. Zou, and F. Xiu, Adv. Mater. **26**, 7110 (2014).

[22] B. A. Piot, W. Desrat, D. K. Maude, M. Orlita, M. Potemski, G. Martinez, and Y. S. Hor, Phys. Rev. B **93**, 155206 (2016).

[23] M. Bianchi, D. Guan, S. Bao, J. Mi, B. B. Iversen, P. D. C. King, and P. Hofmann, Nat. Commun. **1**, 128 (2010).

[24] P. D. C. King, R. C. Hatch, M. Bianchi, R. Ovsyannikov, C. Lupulescu, G. Landolt, B. Slomski, J. H. Dil, D. Guan,

J. L. Mi, E. D. L. Rienks, J. Fink, A. Lindblad, S. Svensson, S. Bao, G. Balakrishnan, B. B. Iversen, J. Osterwalder, W. Eberhardt, F. Baumberger, and P. Hofmann, Phys. Rev. Lett. **107**, 096802 (2011).

[25] M. S. Bahramy, P. D. C. King, A. de la Torre, J. Chang, M. Shi, L. Patthey, G. Balakrishnan, P. Hofmann, R. Arita, N. Nagaosa, and F. Baumberger, Nat. Commun. **3**, 1159 (2012).

[26] B. C. Park, T.-H. Kim, K. I. Sim, B. Kang, J. W. Kim, B. Cho, K.-H. Jeong, M.-H. Cho, and J. H. Kim, Nat. Commun. **6**, 6552 (2015).

[27] P. Syers and J. Paglione, Phys. Rev. B **95**, 045123 (2017).

[28] N. Bansal, Y. S. Kim, E. Edrey, M. Brahlek, Y. Horibe, K. Iida, M. Tanimura, G.-H. Li, T. Feng, H.-D. Lee, T. Gustafsson, E. Andrei, and S. Oh, Thin Solid Films **520**, 224 (2011).

[29] R. V. Aguilar, A. V. Stier, W. Liu, L. S. Bilbro, D. K. George, N. Bansal, L. Wu, J. Cerne, A. G. Markelz, S. Oh, and N. P. Armitage, Phys. Rev. Lett. **108**, 087403 (2012).

[30] E. K. de Vries, A. M. Kamerbeek, N. Koirala, M. Brahlek, M. Salehi, S. Oh, B. J. van Wees, and T. Banerjee, Phys. Rev. B **92**, 201102 (2015).

[31] J. Dai, W. Wang, M. Brahlek, N. Koirala, M. Salehi, S. Oh, and W. Wu, Nano Res. **8**, 1222 (2015).

[32] M. Brahlek, N. Koirala, M. Salehi, J. Moon, W. Zhang, H. Li, X. Zhou, M.-G. Han, L. Wu, T. Emge, H.-D. Lee, C. Xu, S. J. Rhee, T. Gustafsson, N. P. Armitage, Y. Zhu, D. S. Dessau, W. Wu, and S. Oh, Phys. Rev. B **94**, 165104 (2016).

[33] See Supplemental Material at http://link.aps.org/supplemental/10.1103/PhysRevB.96.045433 for details regarding the analysis procedure, magnetotransport measurements for larger thicknesses, AFM images of the grown films, Berry phase determination for $t = 10$ QL, and the values for the extracted charge-carrier densities from the SdH oscillations.

[34] H. Köhler and A. Fabbicius, Phys. Status Solidi B **71**, 487 (1975).

[35] H. Köhler and E. Wöchner, Phys. Status Solidi B **67**, 665 (1975).

[36] A. Wolos, S. Szyszko, A. Drabinska, M. Kaminska, S. G. Strzelecka, A. Hruban, A. Materna, M. Piersa, J. Borysiuk, K. Sobczak, and M. Konczykowski, Phys. Rev. B **93**, 155114 (2016).

[37] M. Orlita, B. A. Piot, G. Martinez, N. K. Sampath Kumar, C. Faugeras, M. Potemski, C. Michel, E. M. Hankiewicz, T. Brauner, Č. Drašar, S. Schreyeck, S. Grauer, K. Brunner, C. Gould, C. Brüne, and L. W. Molenkamp, Phys. Rev. Lett. **114**, 186401 (2015).

[38] B. Fauqué, N. P. Butch, P. Syers, J. Paglione, S. Wiedmann, A. Collaudin, B. Grena, U. Zeitler, and K. Behnia, Phys. Rev. B **87**, 035133 (2013).

[39] C. Martin, V. Craciun, K. H. Miller, B. Uzakbaiuly, S. Buvaev, H. Berger, A. F. Hebard, and D. B. Tanner, Phys. Rev. B **87**, 201201 (2013).

[40] S. Wiedmann, A. Jost, B. Fauqué, J. van Dijk, M. J. Meijer, T. Khouri, S. Pezzini, S. Grauer, S. Schreyeck, C. Brüne, H. Buhmann, L. W. Molenkamp, and N. E. Hussey, Phys. Rev. B **94**, 081302 (2016).

[41] K. Eto, Z. Ren, A. A. Taskin, K. Segawa, and Y. Ando, Phys. Rev. B **81**, 195309 (2010).

[42] L. Veyrat, F. Iacovella, J. Dufouleur, C. Nowka, H. Funke, M. Yang, W. Escoffier, M. Goiran, B. Eichler, O. G. Schmidt, B. Büchner, S. Hampel, and R. Giraud, Nano Lett. **15**, 7503 (2015).

[43] L. Wu, W.-K. Tse, M. Brahlek, C. M. Morris, R. Valdés Aguilar, N. Koirala, S. Oh, and N. P. Armitage, Phys. Rev. Lett. **115**, 217602 (2015).

[44] M. Brahlek, N. Koirala, M. Salehi, N. Bansal, and S. Oh, Phys. Rev. Lett. **113**, 026801 (2014).